REVIEW

Chinese Journal of Structural Chemistry

A Review on Crystalline Porous MOFs Materials in Photocatalytic Transformations of Organic Compounds in Recent Three Years

Hao Zhang[1†], Ru Sun[1†], Da-Cheng Li[1] and Jian-Min Dou[1*]

[1]*Shandong Provincial Key Laboratory of Chemical Energy Storage and Novel Cell Technology, School of Chemistry and Chemical Engineering, Liaocheng University, Liaocheng, Shandong 252059, China*

ABSTRACT Metal-organic frameworks (MOFs) have always been the focus of chemists due to their diverse structures, adjustable pore size and high stability since they came into being. In recent years, as one of the most significant applications of MOFs porous materials, photocatalytic organic compounds transformation has made full-grown progress both in the preparation of the catalysts themselves and in the scope of specific applications. Herein, we summarize the research progress of MOFs catalysts for photocatalytic transformations of organic compounds in recent three years. Some outstanding works on the preparation and synthesis strategies of photocatalysts are introduced firstly, including internal optimization and modification of MOFs, POM@MOF composite and core-shell MOF@COF hybrids. The second part is about the application of diverse types of organic reactions, including dual-function organic reactions, catalytic oxidation reactions, comprehensive utilization of CO_2 and degradation of organic pollutants. Besides, the development opportunities and some problems to be solved in this field are proposed.

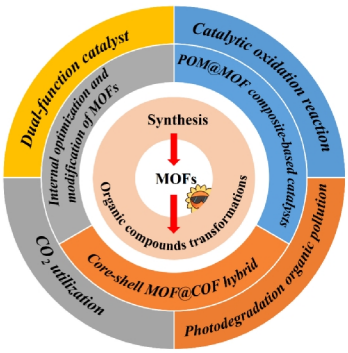

Keywords: metal-organic frameworks, porous materials, photocatalytic reaction, organic transformations

n INTRODUNTION

Photocatalysis is considered as one of the most ideal ways to store and utilize solar energy, so it has attracted extensive attention from all over the world.[1-4] Compared with the traditional thermal catalysis, the photocatalytic transformation of organic compounds has the advantages of mild conditions, friendly environment, high product yield and selectivity, so as to show a unique charm.[5-7] Especially, in the synthesis and conversion of small molecular organics, a large number of scientific articles and literature reports have confirmed the hot spot.[8-15] With the in-depth study of the basic theory of photophysics and photochemistry, many kinds of catalytic materials with good photocorresponding have emerged, including metal sulphides,[16-18] metal oxides,[19-21] metal nitrides[22-25] and some metal-free catalysts. Nevertheless, these classical semiconductor materials have encountered great difficulties in practical application, despite their advantages of low toxicity, low cost and high stability. As far as TiO_2 is concerned, it is known as the photocatalyst with the most potential for commercialization. However, TiO_2 can only absorb ultraviolet light and be excited, which is obviously not satisfactory for the full utilization of solar energy. Alternatively, CdS with high utilization efficiency of visible light is limited by large-scale practical application due to its serious photocorrosion. Although the emerging C_3N_4 material can overcome almost all of the above-mentioned shortcomings, the low quantum yield still makes further researches challenging.

Over the 3 decades, MOFs have attracted much attention because of the structural variability and adjustability, as well as their potential applications in gas storage and separation,[26-30] fluorescence sensing,[31-33] photocatalysis[34-39] and electrocatalysis.[40-44] The infinite variability of MOFs structure is mainly caused by the combination diversity of ligands and metal ions, and the ligands and metal ions play different roles in the reaction process, which makes it the most common method to regulate the optical properties of MOFs by reasonably adjusting internal structure. In addition, MOFs have extremely high specific surface area, ultrahigh porosity and open channels, which allow more catalytic active sites to be exposed and bind to substrate molecules more easily. Although most MOFs have stable frames, they have weak light absorption on their own especially in the visible and near infrared regions. Hence, the organic integration of photosensizers or catalysts and MOFs can not only play the advantages of stable structures of MOFs, but also vastly improve the utilization rate of catalysts fixed at the specific position on the MOFs skeleton. Until now, due to the variable size of the pores in disparate MOFs, the intricate bond relationships between the MOFs and other loaded materials, and diverse mechanisms of various catalytic reactions, the construction of visible-light-responsive MOFs-based mutilcomponent materials with excellent catalytic activity and stability for organic conversion remains challenging and strategic. Alternatively, due to the high cost of ligands themselves and the complicated synthesis process, the progress from laboratory to industrial application is greatly hindered. Finding cheaper ligands with high versatility and mild synthesis methods is significant factors for further application of MOFs materials.

In this review, we summarize the progress of MOFs catalysts in the field of photocatalytic organic synthesis in the past three years, including some innovative and novel synthetic strategies of MOFs and their derivatives, breakthroughs in organic reaction types and prospects for the further development of similar materials. We hope that this review can help readers to have a deeper understanding of MOFs-based materials in photocatalytic or-

Chin. J. Struct. Chem. **2022**, 41, 2211071-2211083
DOI: 10.14102/j.cnki.0254-5861.2022-0140

ganic synthesis, so as to guide and promote further relevant researches.

n SYNTHETIC STRATEGIES OF MOFs MATERIALS

Internal Optimization and Modification of MOFs

Confinement Effects. In addition to being shape-selective for reactants/products, the confinement effects can also regulate the surface electron distribution of active substances in porous environments, thereby affecting the catalytic activity, selectivity and stability in turn.[45-49]

In an example on MOF-based oxidative transformations, Jiang et al. assembled Ir^{III} photocatalyst and Pd^{II} catalyst respectively at spatially proximate positions on MOF, and obtained Pd/photoredox catalysts UiO-67-Ir-PdX_2 (X = OAc, TFA).[50] This new strategy addressed the reoxidation problem of Pd with low valence. As shown in Figure 1a, the Pd and Ir catalysts at the monatomic site were stabilized by the framework of MOFs and were spatially adjacent to each other, which provided preemptive conditions for fast electron transfer. The turnover performance of the as-prepared bimetallic catalysts in decarboxylative coupling reactions was 25 times higher than that of the existing Pd catalysis systems. In terms of mechanism investigations, the single-site Pd in MOF could effectively inhibit the agglomeration of Pd^0, and then promoted the reoxidation of Pd-catalyzed reactions (Figure 1b).

Linker Installation. Precise placement of multiple functional groups in a highly ordered MOF platform enables customizing the pore environment, which is required for advanced applications. Through the linker installation, systematic variation of the pore volume and decoration of pore environment are realized, thus affecting its catalytic performance.[51-55]

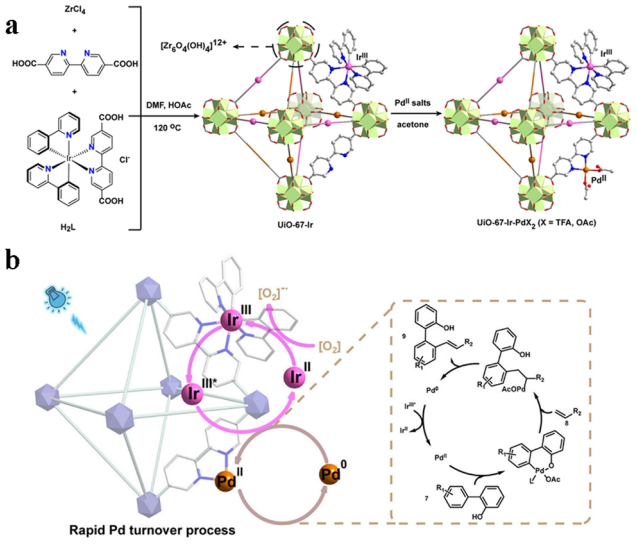

Figure 1. (a) The synthetic diagram of UiO-67-Ir-PdX_2 (X = OAc, TFA), which was synthesized via pre-functionalization and post-synthetic modification. (b) A possible mechanism for the MOFs-based Pd/photoredox catalysis. The C-H alkenylation of 2-phenylphenol catalyzed by this Pd-catalyst was taken as an example. Reproduced with permission from Ref.[50]

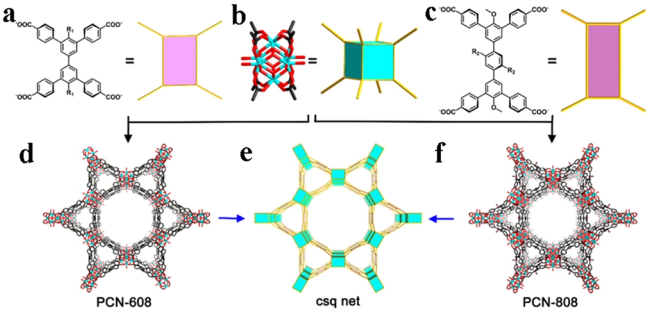

Figure 2. Construction of PCN-608 and PCN-808. (a) The planar and rectangular tetratopic ligand of PCN-608. (b) The Zr_6 cluster in PCN-608 and PCN-808. (c) The expanded planar and rectangular ligand of PCN-808. (d) The crystal structure of PCN-608 (along the *c* axis). (e) The topology structure of mesoporous MOFs PCN-608 and PCN-808. (f) The crystal structure of PCN-808 (along the *c* axis). Color distribution: C, black; O, red; Zr, blue; R_1 on the ligands. R_1 = OH, NH_2 or OMe, R_2 = H or CF_3. Reproduced with permission from Ref.[56]

In 2020, Zhou and his co-workers designed and synthesized a novel Zr_6 clusters based mesoporous MOF, named PCN-808 (Figure 2).[56] In PCN-808, a linear Ru-based ligand was successfully and preciously mounted on the open channel wall via the linker installation while maintaining the mesoporous properties of the framework. The photocatalytic performance of as-prepared catalyst PCN-808-BDBR was tested in the aza-Henry reaction and showed high catalytic conversion yields even after 6 cycles (Figure 3). Encouragingly, this mesoporous catalyst also demonstrated all-right yields for the oxidation of dihydroartemisinic acid to artemisinin under visible light irradiation. The unique and innovative point was that this study provided a basis and guidance for the regulation of controlling pore environment in mesoporous MOFs. In the same year, Zhou incorporated multifunctionalities into MOLs through secondary ligand pillaring (ditopic and tetratopic linkers).[57] Notably, the metal-phthaloyanine was successfully incorporated to the Zr-MOL system (Figure 4a),

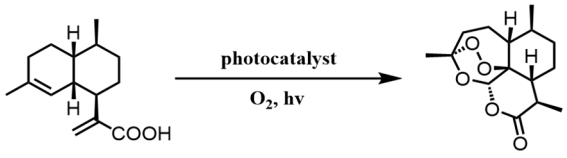

catalyst	conversion (%) / yield (%)[a] run 1	run 2	run 3
$Ru(bpy)_3Cl_2$	>99/47	N.A	N.A
PCN-808	<5/<5	N.A	N.A
UiO-67-Ru	30/<5	N.A	N.A
PCN-808-BDBR	**92/42**	**88/51**	**90/49**

Figure 3. Oxidation of dihydroartemisinic acid to artemisinin catalyzed by PCN-808-BDBR under visible light irradiation. [a]The conversion yields of the product were determined by ^1H NMR. Reproduced with permission from Ref.[56]

DOI: 10.14102/j.cnki.0254-5861.2022-0140

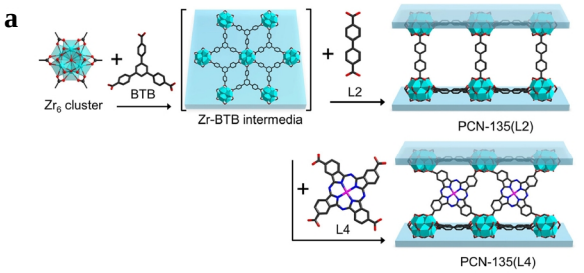

Entry	R	Catalyst	Yield [%][b]
1	H	PCN-135(Co-TCPc)	95
2	Me	PCN-135(Co-TCPc)	92
3	H	PCN-135(Co-TCPc)[c]	92
4	H	PCN-135(Co-TCPc)[d]	NR[e]
5	H	PCN-135(Co-TCPc)[f]	NR
6	H	Co-TCPc	60
7	H	Co-TCPc[g]	26
8	H	_[h]	NR

Figure 4. (a) The synthesis diagram of the PCN-135 family. Zr_6-BTB was appointed as the precursor and a series of linear ligands or tetratopic ligands as the secondary ligands. (b) The catalytic oxidation reaction of anthracene to anthraquinone. Reproduced with permission from Ref.[57]

which was appointed as an efficient heterogeneous catalyst for the selective anthracene oxidation. This work not only introduced a novel strategy for incorporating phthalocyanine fragments, but also opened the door to design new 2D molecular functionalities materials (Figure 4b).

POM@MOF Composite-Based Catalysts

The combination of MOFs and POMs addresses the advantages

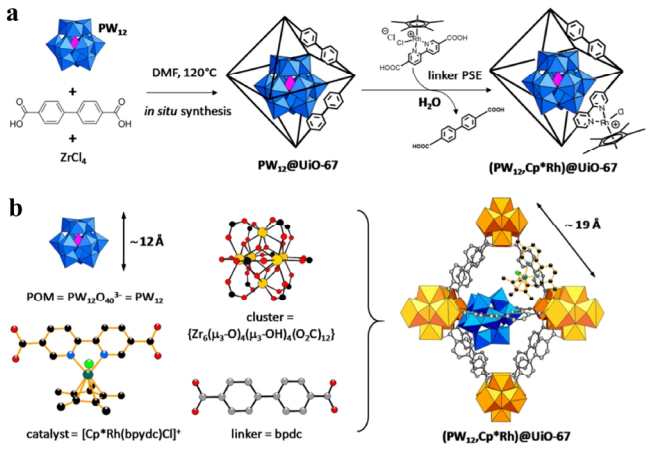

Figure 5. (a) The schematic diagram of two-step *in situ* synthesis of (PW_{12},Cp*Rh)@UiO-67 and postsynthetic exchange (PSE) procedure of linkers. (b) The components of (PW_{12},Cp*Rh)@UiO-67: the PW_{12} POM, the subunit of UiO-67 Zr-based MOF, the $[Cp^*Rh(bpydc)Cl]^+$ Rh-based molecular catalyst and the bpdc linkers. Density functional theory (DFT) calculations were used to give the specific position of POM (see the original text). Reproduced with permission from Ref.[64]

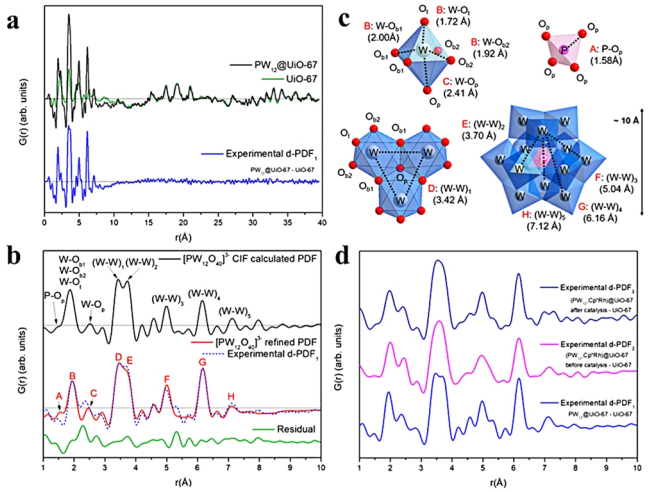

Figure 6. (a) The experimental PDF of PW_{12}@UiO-67 (black curve) and UiO-67 (green curve), and the related d-PDF for PW_{12}@UiO-67 (blue curve). (b) The comparison of $[PW_{12}O_{40}]^{3-}$ CIF calculated PDF (black curve), $[PW_{12}O_{40}]^{3-}$ refined PDF obtained from the CIF file JCPDS 00-050-0304 (blue dotted curve), experimental d-PDF (red curve) and residual profile (green curve). (c) The refined distances for the PO_4 tetrahedron, the WO_6 octahedron, the trimer of WO_6 octahedra and the full PW_{12} polyoxometalate structure in the POM components. (d) Experimental d-PDFs (1-3) of PW_{12} in PW_{12}@UiO-67 (blue curve), in (PW_{12},Cp*Rh)@UiO-67 before (magenta curve) and after (navy curve) catalysis. Reproduced with permission from Ref.[64]

of POM and MOFs while avoiding their respective disadvantages. MOFs with high specific surface area and long range ordered structure make uniform distribution of POMs possible, which can not only prevent self-aggregation of POMs, but also expose more active sites for catalytic reactions.[58-63] These composites are considered as promising photocatalytic materials due to their unique advantages, such as ultra-high porosity, large specific surface area and better electron redox conversion.

In an article on the utilization of CO_2, Caroline's research group *in situ* integrated the UiO-67 MOF and Keggin-type $PW_{12}O_{40}^{3-}$ POM, and then introduced Rh-based catalyst $Cp^*Rh(bpydc)Cl_2$ (bpydc = 2,2'-bipyridine-5,5'-dicarboxylic acid) by postsynthetic linker exchange (Figure 5).[64] The photocatalytic performance of obtained (PW_{12}, Cp*Rh)@UiO-67 POM@MOF composite for CO_2 reduction into formate was measured under visible light irradiation. Compared with the POM-free Cp*Rh@UiO-67 catalyst, the formate production was doubled and the TON was as high as 175. Intriguingly, the authors proposed an extremely robust structural assessment of Cat@MOFs based on differential Pair Distribution Function (d-PDF) results, which was related to a computational Monte Carlo/DFT approach. The d-PDF analysis assisted in verifying the integrity of POM before and after the catalysis (Figure 6).

Core-Shell MOF@COF Hybrids

By introducing the prepared MOFs into the synthesis of COFs, a new type of core-shell hybrid MOF@COF material was cons-

DOI: 10.14102/j.cnki.0254-5861.2022-0140

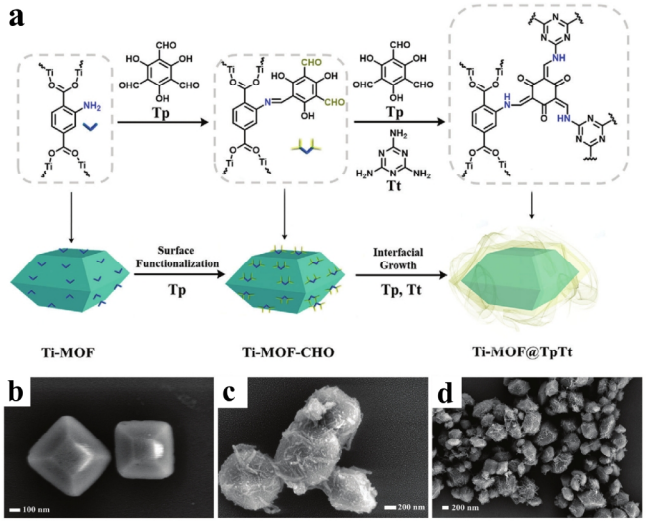

Figure 7. (a) The synthesis illustration of the Pd decorated Ti-MOF@TpTt catalyst. The SEM images of the (b) Ti-MOF and (c, d) Ti-MOF@TpTt. Reproduced with permission from Ref.[70]

tructed. Not only did it inherit the high specific surface area of the parent porous MOF and COF materials, but also the existing spatial separation and strong covalent connection between MOF and COF could effectively promote the charge transfer between the two components, which made the core-shell MOF@COF hybrid have excellent photocatalytic activity.[65-69]

Zang and his co-authors successfully synthesized a Ti-MOF@TpTt hybrid material coated with ultrathin COF nanoribbons via continuous growth strategy (Figure 7a).[70] Different from the fibrous structure of massive COF, this TpTt COF can grow vertically on the Ti-MOF surface and form ultra-thin nanoribbon through regulating the amount of ligands. SEM results revealed that the truncated bipyramid octahedral structure of Ti-MOF remained in the Ti-MOF@TpTt composite after surface functionalization (Figure 7b-d). The *in situ* construction of Pd decorated Ti-MOF@TpTt catalyst presented outstanding performance in the photocatalytic cascade reactions of ammonia borane (AB) hydrolysis and nitroarenes hydrogenation. The authors pointed out three reasons for the excellent properties of the composite. Firstly, the formation of Type-II heterojunction promoted the separation of carriers. Secondly, the core-shell structure further promoted the separation of photogenerated electrons at the spatial level. Thirdly, the ultra-thin COF nanoribbon shell structure for loading Pd NPs was conductive to exposing more active sites and reducing the migration distance of the reaction matrix.

n APPLICATIONS OF MOFS MATERIALS IN PHOTOCATALYTIC ORGANIC TRANSFORMATIONS

Dual-Function Catalyst. Tandem reactions improve resource utilization and reduce waste generation by performing multiple organic transformations in a single synthetic operation without the need to separate and purify specific reaction intermediates produced at each step.[71-76]

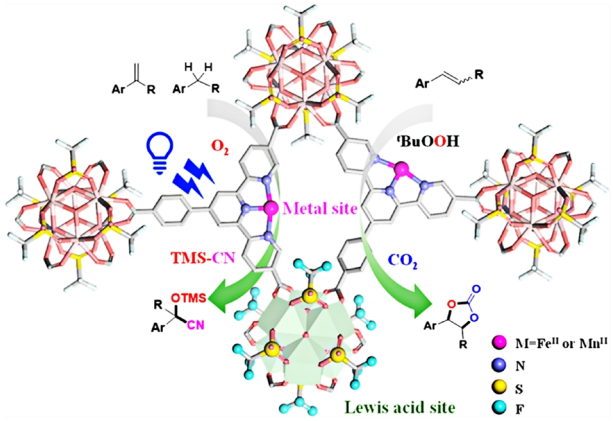

Figure 8. The tandem catalytic schematic diagram of the bifunctional MOLs containing Hf_6 SBUs Lewis acidic and TPY-M (M = Fe^{II} of Mn^{III}) ligands. Reproduced with permission from Ref.[77]

Lin et al. reported the design of a dual-functional layered MOF material, HfOTf-Fe and HfOTf-Mn, in which Hf_6 secondary building units (SUBs) capped by trifluoromethanesulfonic acid (OTF) were used as strong Lewis acid sites (Figure 8).[77] Moreover, the 4'-(4-carboxyphenyl) [2,2':6',2"-terpyridine]-5,5"-dicarboxylate (TPY) ligands can be appointed as active sites for metal catalysis. It was found that HfOTf-Fe effectively transformed hydrocarbons into cyanohydrins by tandem oxidation with O_2 and silycyanation, while HfOTf-Mn converted styrenes into styrene carbonates by tandem epoxidation and CO_2 injection (Figure 9a-b). Density functional theory calculations revealed that the high spin Fe^{IV} was involved in the oxidation of the sp^3 C-H bond (Figure 9c-d). This work not only realized the tandem catalytic reaction of O_2 and CO_2 as reactants, but also reported for the first time the synthesis of cyanohydrin from aromatic alkanes.

Catalytic Oxidation Reaction. As one of the most classical and diverse reactions in organic chemistry, catalytic oxidation is more promising due to its combination and mutual use with solar energy. Some reactions under extreme conditions are softened

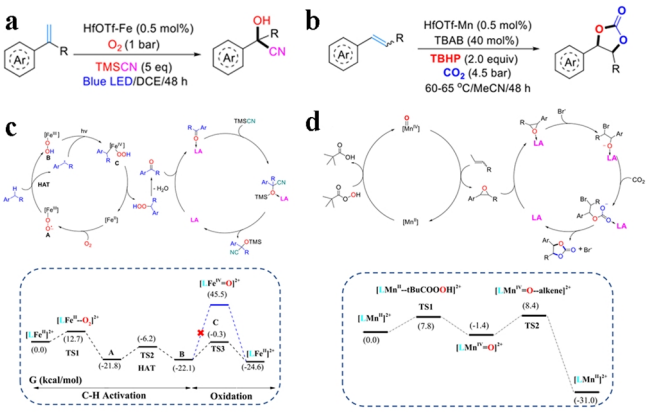

Figure 9. (a) Cyanohydrination reaction for tandem oxidation of hydrocarbons based on HfOHf-Fe catalyst and (c) its corresponding proposed mechanism. (b) CO_2 insertion of styrenes reaction for tandem epoxidation based on HfOHf-Mn catalyst and (d) its corresponding proposed mechanism. Reproduced with permission from Ref.[77]

DOI: 10.14102/j.cnki.0254-5861.2022-0140

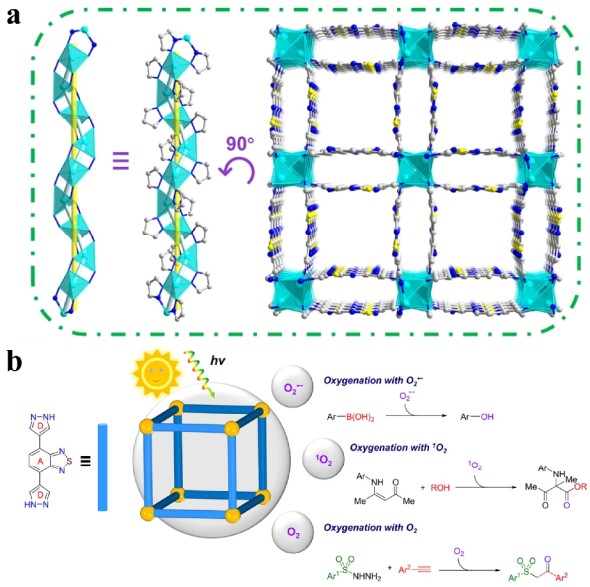

Figure 10. (a) The crystal structure diagram of JUN-204, Zn (sky blue), C (gray), N (blue), O (red). All the H atoms were omitted for clarity. ZnN_4 clusters (cyan tetrahedra) were connected by pyrazole molecules with shared edges to form helical rod SBUs, which were cross-linked via PBT connectors to form a 3D frame with square channels along the [001] direction. (b) Schematic diagram of JUN-204 photocatalyst for aerobic oxygenation upon visible light irradiation. Reproduced with permission from Ref.[78]

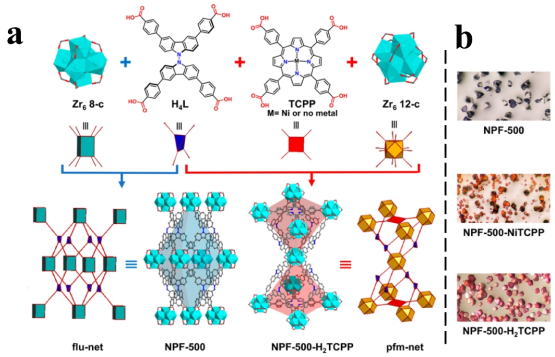

c

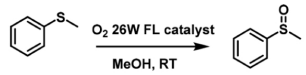

entry	photocatalyst	catalyst loading (%)	conversion (%)
1	NPF-500	0	0
2	NPF-500-H_2TCPP	0.2	99
3	H_2TCPP	0.2	99
4	NPF-500-H_2TCPP	0.2	97[a]
5	PCN-222	0.2	41

[a]Recycled for five times.

Figure 11. (a) The structures of Zr_6 clusters, H_4L and H_2TCPP/NiTCPP, and the formation diagram of NPF-500, NPF-500-H_2TCPP/NiTCPP and their corresponding topological structures (C: gray, O: red, N: blue, Zr: cyan polyhedra). (b) The optical photographs of NPF-500, NPF-500-NiTCPP and NPF-500-H_2TCPP. (c) The oxygenation reaction of thioanisole based on various photocatalysts. Reproduced with permission from Ref.[79]

after the introduction of illumination.

Li et al. reported the development of an organic molecule with pyrazole-benzothiadiazole-pyrazole structure that can be used as a donor-acceptor-donor (D-A-D type) conjugated π-system to achieve superb capability of photon absorption, applicable bandstructure and rapid charge separation (Figure 10a).[78] JNU-204 heterogeneous catalyst with excellent photocatalytic activity was obtained by assembling photosensitizer molecules into MOF material. Under visible light irradiation, JNU-24 MOF realized three aerobic oxidation reactions (Figure 10b), which are arylboronic acid oxidation (oxygenation with $O_2^{\bullet-}$), enamine oxidation (oxygenation with $^1O_2$) and oxysulfonylation of alkynes (oxygenation with O_2). The authors synthesized pyrrolo[2,1-a]-isoquinoline-derivatives (a significant structure of marine natural product molecules) by using the JNU-204 MOF in an uncomplicated pathway, and verified that the high stability and repeatability of JNU-204 through cyclic catalytic experiments. Placing the energy donor and acceptor parts within the same frame with atomic precision seems to be a major synthetic challenge. In another report about the energy donor and acceptor,[79] Zhang et al. designed and synthesized a highly porous and photoactive MOF named NPF-500-H_2TCCP (NPF = Nebraska porous framework, H_2TCPP = *meso*-tetrakis(4-carboxyphenyl)porphyrin). The equatorial plane of the octahedral cage in NPF-500 closely matched the size and the shape of the photoactive porphyrin ligand H_2TCPP, forming an ideal donor-acceptor structure for light harvesting and energy transfer (Figure 11a-b). The NPF-500-H_2TCCP could selectively oxidize thioanisole to the relevant sulfoxide with a 99% yield in 1 h and exhibited excellent cyclic stability (five times without obvious decrease) (Figure 11c). This work might provide a new blueprint for the design of high-efficient light-harvesting and energy transfer capability systems.

In another reported oxidative coupling reaction of amine compounds, p-TCN@UiO-66-NH_2 catalyst was synthesized via *in situ* loading of UiO-66-NH_2 on the surface of p-TCN (phospho-

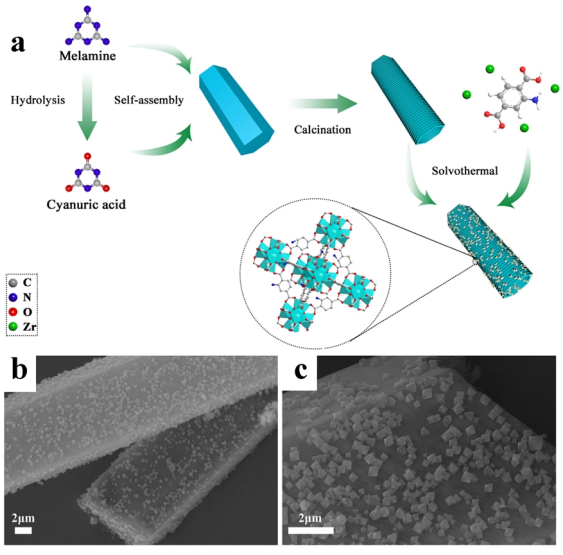

Figure 12. (a) The synthesis diagram of the p-TCN@U6-X. (b-c) SEM images of p-TCN@U6-3. Reproduced with permission from Ref.[80]

DOI: 10.14102/j.cnki.0254-5861.2022-0140

rus-doped tubular carbon nitride) (Figure 12).[80] The composite exhibited 99% selectivity rate and 98% conversion rate for coupling reaction of benzylamine. In addition, the H_2 evolution rate of p-TCN@U6-3 could achieve 2628 μmol g^{-1} h^{-1} under visible light irradiation, which is 5.36 and 8.19 times higher than that of pure UiO-66-NH_2 and p-TCN. Such materials with both photocatalytic oxidation and reductive properties are rare and therefore are expected to be further developed in the fields of energy, environment and biomedicine.

The reaction process was greatly influenced by the inorganic-organic interface between metal catalysts and the substrates. Zhu et al. discovered the functionalization reaction of catalytic oxidation excited by NIR light through ligand modification, thus improving the photocatalytic performance of Au nanoclusters (Figure 13a).[81] Notably, they found that increasing the stiffness of the protected ligand geometry effectively prevented the deformation of the metal core due to the Jahn-Teller effect. To investigate the potential for future industrial applications, the authors expanded the equivalent by 50 times and compared the performance between the blue LED light and near-infrared light with the same power (3 W). When the 460 nm blue LED light was used as the light source, the synthesis yield was only 69% within 48 h. Correspondingly, a supernal 99% yield of product was obtained in 8 h when using an 850 nm LED (Figure 13b). These meaningful results revealed possible application value for near-infrared photocatalysis in future industry.

CO_2 Utilization. With continuous deterioration of global greenhouse effect, the comprehensive correlation researches based

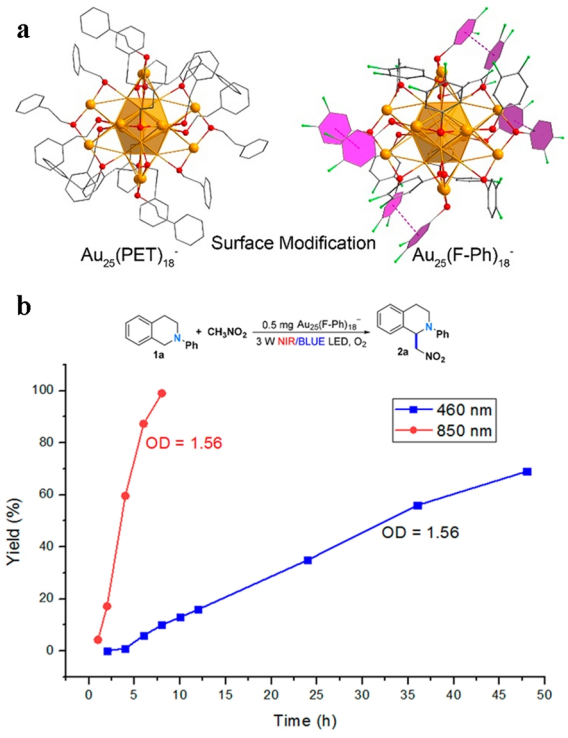

Figure 13. (a) The structures of $Au_{25}(PET)_{18}^-$ and $Au_{25}(F\text{-}Ph)_{18}^-$. (b) The synthesis yield via using $Au_{25}(F\text{-}Ph)_{18}^-$ with NIR and blue LED light against with time. Reproduced with permission from Ref.[81]

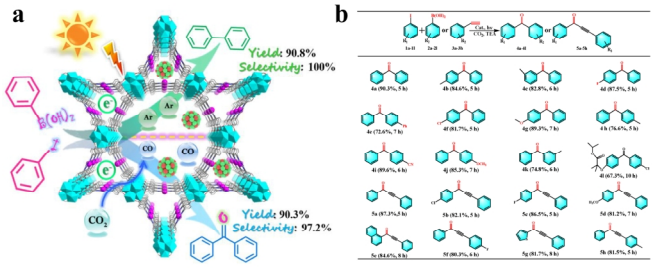

Figure 14. (a) Multicomponent synergistic effects of $(Cu_1Pd_2)_{1.3}$@PCN-222(Co) photocatalyst for visible-light-driven Suzuki coupling reaction under CO_2 or Ar. (b) Carbonylation reaction of different aryliodides upon visible light irradiation. Reproduced with permission from Ref.[89]

on CO_2 increased sharply. Whether the rational utilization of CO_2 can be realized is a vital strategic point for improving climate and living environment in the 21th century.[82-84] Due to the high symmetry and difficulty to activate the CO_2 molecule, conventional single metal catalysts or MOFs materials have not performed well either in the reduction reaction of CO_2 itself or as reactions involved in other reactions such as CO_2 cycloaddition or specific organic coupling reactions. This appearance promoted researchers to carry out in-depth study on the combination of multi-component, polycrystalline or multi-phase catalysts.[85-88]

It makes sense to use CO_2 instead of toxic CO as C1 source for solar-driven carbonylation reactions, but this is still an untoward challenge due to the high inertia of CO_2 molecules themselves. Based on this, Zhang and his co-authors reported that a series of composite photocatalysts $(Cu_1Pd_2)_z$@PCN-222(Co) (z = 1.3, 2.0, and 3.0 nm) were constructed by integrating cobalt single-site and ultrafine CuPd nanoclusters onto a porphyrin-based MOF (Figure 14a).[89] Upon visible-light irradiation, the excited porphyrins can transfer electrons to Co single-site and ultrafine CuPd nanoclusters simultaneously. In the presence of CO_2, the photosynthesis of benzophenone was significantly improved via synergistic effects of multiple components in $(Cu_1Pd_2)_{1.3}$@PCN-222(Co), with a yield higher than 90% and a selectivity more than 97% (Figure 14b). It is noteworthy that the famed cholesterol-lowering pharmaceutical molecule fenofibrate was synthesized for the first time under mild and environmentally friendly conditions in this $(Cu_1Pd_2)_{1.3}$@PCN-222(Co)-based photocatalytic system.

In another example of CO_2 utilization, a robust composite catalyst ZIF-8@Au_{25}@ZIF-67[tkn] (tkn was the thickness of shell) was successfully constructed via coordination-assisted self-assembly by Zhu and co-authors and this was the first report of APNC decorative MOF materials with sandwich-like structure (Figure 15a).[90] Fortunately, the shell thickness of ZIF-8@Au_{25}@ZIF-67[tkn] could be controlled arbitrarily by precisely adjusting the concentration of 2-MeImA and Co^{2+} added. The carboxylation reaction of terminal alkyne was appointed as the model example to test the as-prepared catalysts. Under optimal conditions, the ZIF-8@Au_{25}@ZIF-67[12] has superior performance to others, which maintained 99% conversation yields even after 3 cycles. In Figure 15b, authors gave the possible mechanism for carboxylation. Step 1: under the combined action of Cs_2CO_3 and Au_{25}, the

DOI: 10.14102/j.cnki.0254-5861.2022-0140

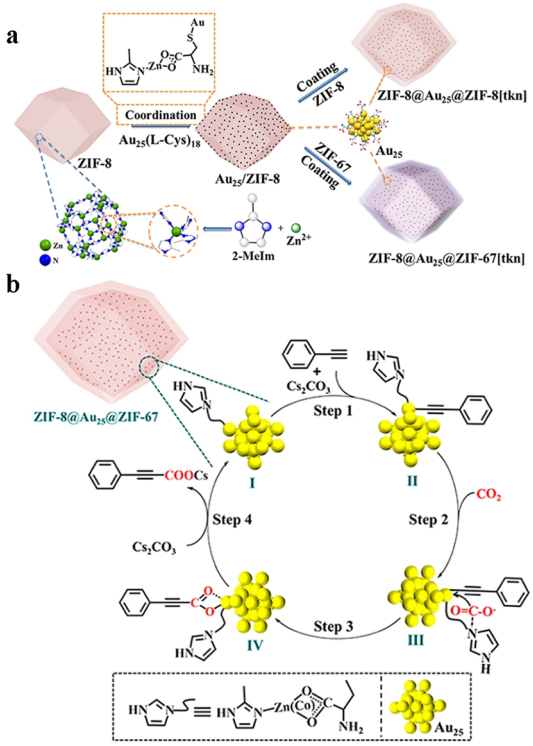

Figure 15. (a) The synthetic procedure of ZIF-8@Au_{25}@ZIF-8[tkn] and ZIF-8@Au_{25}@ZIF-67[tkn] with sandwich structures, and [tkn] was the thickness of shell. (b) Possible reaction mechanism between terminal alkynes and CO_2 for ZIF-8@Au_{25}@ZIF-67[tkn]. Reproduced with permission from Ref.[90]

intermediate II formed. Step 2: CO_2 molecule was captured by the 2-MIem in the ZIF-67 shell and led the formation of intermediate III. Step 3: the activated CO_2 molecule inserted to the bond of C≡C···Au and gave the intermediate IV. Step 4: the products were formed and the catalyst was regenerated, so that a complete catalytic process could continue. Hence, this highly artistic work will stimulate chemists' interest in designing sandwich-like structure composites MOF@APNC@MOF with excellent photocatalytic properties, and open up a new research direction for the expansion of nano-metal and MOFs materials.

In addition to the above-mentioned two examples of CO_2 indirectly participating in organic reactions, the photocatalytic reduction of CO_2 itself to methane and formats and other organic compounds had also made extraordinary substantial progress. Noble metal nanoparticles (NPs), especially Pd and Ru based NPs, have been extensively studied in the CO_2 methanation reactions. At the same time, non-noble metal Fe, Co, Ni based NPs also emerged in an endless stream. However, the nature of metal NPs was not the only factor determining catalytic performance. The thermal and optical properties of the carrier also played a very significant role. Jorge's group reported the synthesis of a highly active and stable MOF derived Ni-based catalyst (Ni-MOF-74) for the photothermal reduction of CO_2 to CH_4 (Figure 16a).[91] Through controlled pyrolysis of MOF-74 (Ni), the photothermal properties of carbon can be adjusted. Under optimal conditions, the methane yield is 488 mmol g^{-1} h^{-1} and no

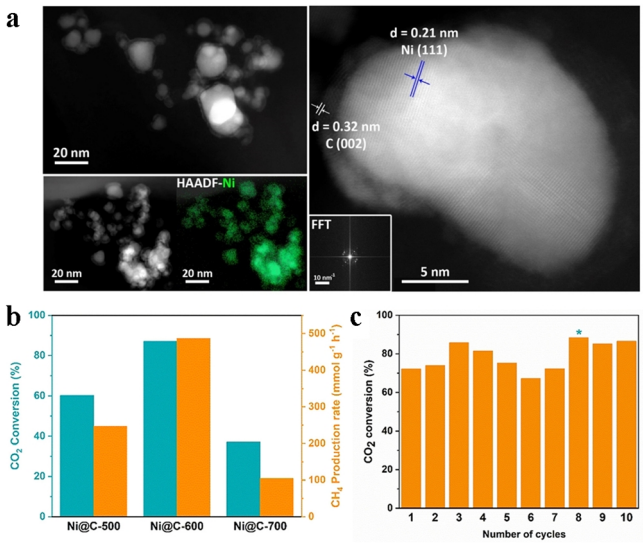

Figure 16. (a) STEM images of Ni@C-600 and STEM mapping. (b) The CO_2 conversion and CH_4 production rates of Ni@C-500, Ni@C-600 and Ni@C-700. (c) The CO_2 conversion against with the catalytic cycles. Reproduced with permission from Ref.[91]

particle aggregation or apparent activity loss is observed in 10 cycles (Figure 16b-c). Intriguingly, the researchers conducted outdoor experiments under direct sunlight, demonstrating the potential of the catalysts to achieve CO_2 methanation using only solar energy. In the field of CO_2 reduction to produce hydrocarbons, Zhang and colleagues reported the preparation of a series of catechol metalloporphyrins, (In/Fe)TCP-Co and (In/Fe)TCP-OH-Co acid and alkali resistant frameworks (Figure 17).[92] Experimental results and density functional theory calculations manifested that the iron-oxygen chains in FeTCP-Co were more favorable for photogenerated electron-hole separation than the indium-oxygen chains in InTCP-Co. After introducing uncoordinated hydroxyl groups into FeTCP-Co, the interaction between CO_2 and photocatalyst was reinforced, so as to enhance the photogenerated carrier transfer. The synergistic effect made FeTCP-OH-Co have the highest CO_2 reduction rate. These MOFs derivatives can perform CO_2 reduction reaction under visible light

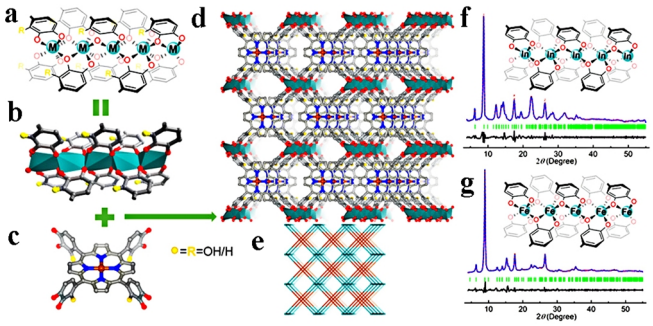

Figure 17. (a, b) The coordination chain of In/Fe-(hydroxy)catechol. (c) The (hydroxy)catechol-metalloporphyrin ligand. Structures of (In/Fe)TCP-Co (d) and (In/Fe)TCP-OH-Co (e). The as-synthesized and Rietveld-refined PXRD patterns of InTCP-Co (f) and FeTCP-Co (g). Reproduced with permission from Ref.[92]

DOI: 10.14102/j.cnki.0254-5861.2022-0140

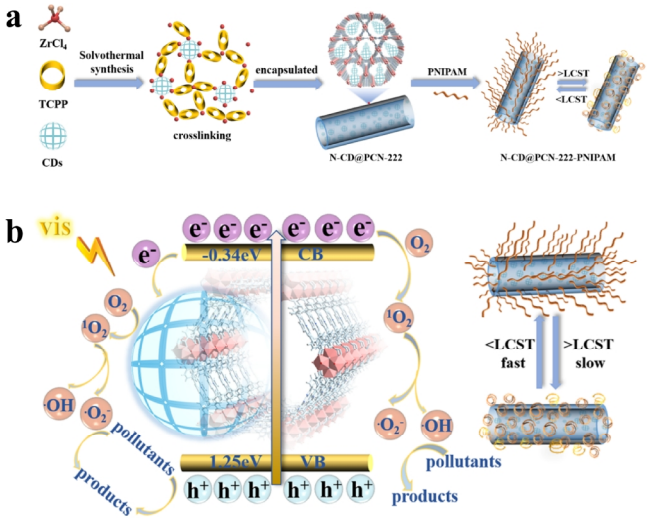

Figure 18. (a) The schematic diagram of N-CDs@PCN-222@PNIPAM photocatalyst. (b) The possible mechanism for the degradation of RhB and TC based on 2N-CDs@PCN-222@PNIPAM$_2$ upon visible-light irradiation. Reproduced with permission from Ref.[98]

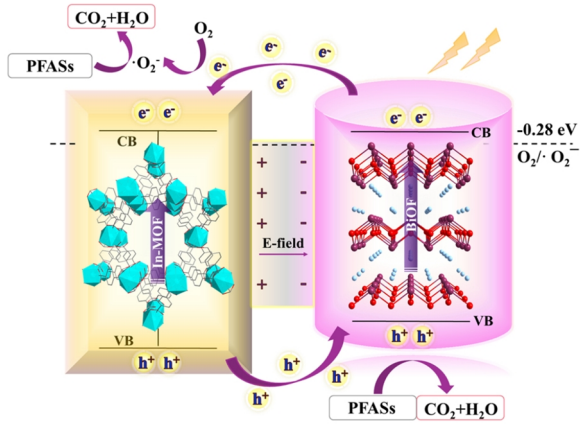

Figure 19. The proposed mechanism for In-MOF/BiOF degradation system under visible-light irradiation. Reproduced with permission from Ref.[99]

irradiation without adding any photosensitizers or sacrificial agents. The use of a single component played a multi-component role, which made the heterogeneous photocatalyst a promising application in artificial photosynthesis and provided guidance for the design of efficient photocatalyst.

Photodegradation Organic Pollution. The degradation and transformation of organic pollutants and wastes are one of the problems that researchers in the fields of environment, chemistry and materials have been working on.[93-95] In addition to the pursuit of high degradation rates or conversion yields and broader degradation goals, more detailed design can better meet the requirements of the contemporary background, such as the realization of selective enrichment in reactive active centers and the combination of theories and experiments to explain and deduce the possible mechanism.[96-97]

Lü et al. encapsulated various carbon dots (CDs) into the surface wettability modified PCN-222 nanoporous cells using thermally responsive catechol terminal PNIPAM with different chain lengths (Figure 18a).[98] A porphyrin-based Zr-MOF nanohybrid (CDs@PCN-222@PNIPAM) was successfully prepared as a highly efficient hydrophilic photocatalyst. Due to the electron collecting function of N-doped CDs (N-CDs) and the existence of synergistic effects with PCN-222, the photocatalytic results of the as-prepared photocatalyst were significantly improved. The remarkable degradation and transformation efficiency of RhB and TC reached 100% and 90.93%, respectively, within just 20 min. And most strikingly, the introduction of hygrophilic polymers enhanced the wetting of the photocatalyst surface and improved the dispersibility of the catalysts toward water (Figure 18b), which promoted the enrichment and further transformation of water-soluble target pollutants near the active sites.

Due to the presence of strong C-F bond, the degradation and transformation of poly/perfluoroalkyl substances (PFASs) have always been a difficult problem and great challenge. Recently, Zhu and colleagues selected BiOF and In-MOF as basic materials and prepared a series of In-MOF/BiOF composites through doping.[99] First, the built-in electric field constructed at the interface accelerated the transfer of photogenerated carriers and reverse phase separation, which made the composite have a stronger ability to participate in redox reactions. Second, the In-MOF provided a substrate with strong adsorption and activation of PFASs, which also accelerated the degradation of PFASs (Figure 19). As shown in Figure 20a, within only 150 min, the 20% In-MOF/BiOF catalyst could achieve full degradation (100% conversion yields) of PFOA. Figure 20b reveals the relationship

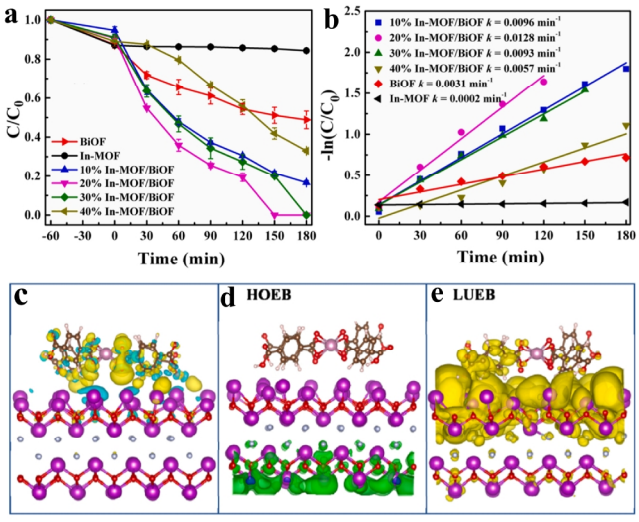

Figure 20. (a) Adsorption and degradation for PFOA against with time. (b) The pseudo-first-order fitting to PFOA of the as-synthesized catalysts. (c) 3D charge density difference of the In-MOF/BiOF photocatalyst (yellow and cyan indicate areas where charge accumulates). (d) The charge density distributions for the energy band of HOEB (green colors indicate the charge density distribution with electron occupation). (e) The charge density distributions for the energy band of LUEB (yellow colors indicate the charge density distribution with electron occupation). Reproduced with permission from Ref.[99]

DOI: 10.14102/j.cnki.0254-5861.2022-0140

between the reaction rate constants k_{obs} (min^{-1}) and the adsorption energy of PFASs on the catalyst. For 20% In-MOF/BiOF catalyst, the parameter k_{obs} was calculated to be 0.0031 min^{-1} according to the formula $-ln(C_t/C_0) = k_{obs} \cdot t$. The charge transfer and redistribution at the interface of In-MOF/BiOF composite system were studied by calculating 3D charge density difference. Relevant results are shown in Figure 20c, where the blue and yellow areas represent the charge accumulation and consumption, respectively. The variation of charge density at the interface showed that the electron transfer from BiOF to In-MOF mainly through the interface and the accumulation of net charges led to the formation of built-in electric field at the In-MOF/BiOF interface. The direction of the electric field was from the In-MOF surface to the BiOF surface, which was favorable for the separation of photogenerated electron-hole pairs. Further calculations of HOEB (the highest occupied energy band) and LUEB (the lowest unoccupied energy band) of the In-MOF/BiOF composite uncovered that the photogenerated electrons at HOEB were easily excited and transited to LUEB (Figure 20d-e). In other words, the photogenerated electrons in BiOF transferred to the in-MOF/BiOF surface interface, and eventually accumulated on the In-MOF surface through the internal electric field, leaving the photogenerated holes on HOEB in BiOF. In this way, the electrons will be far away from the holes, so as to achieve a more effective separation of carriers and improve the photocatalytic performance of the composite.

n CONCLUSIONS AND PROSPECTS

In this review, we summarized the outstanding advances in the field of MOFs-based photocatalytic organic conversion reactions in the last three years. The dominating contents mainly focused on two aspects. The first was the breakthrough in the synthesis of MOFs-based photocatalyst, which mainly introduced novel structure or specific structure-oriented MOFs by means of the internal optimization and modification of MOFs, coupled with POMs and COFs. The second was the concrete application of organic conversion, including dual-function catalysts catalyzed multiple types of efficient organic reactions, catalytic oxidation reaction, cycloaddition of CO_2 and CO_2 reduction, degradation and transformation of organic pollutants. Although the corresponding researches in this area have started late, the accomplishments have been surprising and exciting. This means both opportunities and challenges exist at the same time, and more persistent efforts should be put into promoting the long-term and quality development of this research direction.

(1) In terms of MOFs skeleton, there are few types, mainly concentrated on the Zr,[100,101] Zn[102,103] and Ti MOFs,[104,105] while reports on organic conversion catalyzed by MOFs-based photocatalysts of traditional transition metals such as Fe, Cu and Ni are relatively rare. Alternatively, most of the photosensitizers and cocatalysts embedded or fixed on the skeleton are precious metal complexes such as Pd, Rh and Ir, which makes the reactions not confirm to the principle of economy. Some coordination unsaturated Co and Ni based molecular catalysts also have the potential of photocatalytic oxidation and reduction, but the troublesome problem that these complexes are not easy to recoordinate and inlay into the MOFs skeleton or pores needs to be carefully considered and solved. The introduction of metal complexes such as coordination unsaturated with variable valence states of central ions might make this field more brilliant and diversified. At present, the structural characterization of these MOFs-derived or composite materials is not very distinct, because researchers are often unable to obtain their single crystals. Hence, some advanced optical and spectral characterization methods are particularly important and also need to be developed and popularized.

(2) Reaction stability and cyclic stability are equally crucial, but the two factors are rarely mentioned together in some articles. The rapid transfer of electrons and energy between MOFs and cocatalysts may lead to skeletal collapse or mechanical damage, the agglomeration of materials during recycling and stability in contact with other non-solution media such as air. These factors are very momentous for the evaluation of materials. High reaction stability and cyclic stability are the prerequisite conditions for the MOFs-based photocatalysts to be studied extensively and deeply.

(3) It is necessary to recognize the difference between visible-light driven catalysis and solar driven catalysis, and the visible-light source for laboratory reactions is the 300 W Xe lamp. In addition, the amount of photocatalyst is too slight to achieve gram-scale reaction, which undoubtedly brings some other troubles to the industrial production or larger scale reactions in the future. Therefore, trying to carry out the reactions under real sunlight and enlarging the reaction scale should be two urgent improvement strategies and research directions for industrial practical applications.

(4) We have to admit that there are always some fuzzy points in the study of reaction mechanism. This is related to the complexity of the reaction architecture, including structure-activity relationship, electron transfer between the MOFs framework and the cocatalyst, interaction between the solution and catalysts, and energy transition permission or blocking, etc. More detailed and clearer interpretation of the reaction mechanism may require new characterization techniques, more accurate theoretical simulation[106] and unremitting efforts of researchers, which will lay a solid foundation for the development of the next generation of more efficient and stable MOFs-based photocatalysts in the future.

(5) In most of the examples presented in this paper, the ligands used for MOFs are still very expensive, and the crystal yields are usually no more than 50%. This situation is far from qualified for industrial production which pursues economic benefits and high utilization of atoms. Although some MOFs materials have shown outstanding catalytic performance in the laboratory, how to achieve industrialization to better serve society and benefit mankind is still a long-term focus. In addition, some studies lack control and consideration under sub-optimal experimental conditions, such as pH value, gas atmosphere and reaction vessel specifications. Therefore, some of the necessary attempts are significant. Because each factor is interrelated, it is untoward to ensure that the optimal conditions before and after scaling up are consistent. Finally, for MOFs derivatives and composites, research-

DOI: 10.14102/j.cnki.0254-5861.2022-0140

ers should focus on studying the original driving force that can recombine or coexist between them, including electrostatic attraction, ionic bond and coordination bond, etc.

n ACKNOWLEDGEMENTS

Thanks to the National Natural Science Foundation of China (21701078) for the financial support of this work.

n AUTHOR INFORMATION

Corresponding author. Email: jmdou@lcu.edu.cn (Jianmin Dou)

n AUTHOR CONTRIBUTION

† Hao Zhang and Ru Sun contributed equally to this work.

n COMPETING INTERESTS

All the authors declare that they have no known competing financial interests that could affect the work reported in this article.

n ADDITIONAL INFORMATION

Full paper can be accessed via
http://manu30.magtech.com.cn/jghx/EN/10.14102/j.cnki.0254-5861.2022-0140
For submission: https://www.editorialmanager.com/cjschem

n REFERENCES

(1) Somnath, C.; Oomman, K.; Maggie, P.; Craig, A. Toward solar fuels: photocatalytic conversion of carbon dioxide to hydrocarbons. *ACS Nano* **2010**, 4, 1259-1278.

(2) Lisa, C.; Karl, D.; Gemma, C.; James, J.; Adrián, G.; Anais, J.; Sebastian, K. Photocatalysis in the life science industry. *Chem. Rev.* **2022**, 122, 2907-2980.

(3) Chen, Z.; Zhou, X.; Yi, J.; Diao, H.; Chen, Q.; Lu, G.; Weng, J. Catalytic decarboxylative fluorosulfonylation enabled by energy-transfer-mediated photocatalysis. *Org. Lett.* **2022**, 24, 2474-2478.

(4) Xing, P.; Wu, S.; Chen, Y.; Chen, P.; Hu, X.; Lin, H.; Zhao, L.; He, Y. New application and excellent performance of Ag/$KNbO_3$ nanocomposite in photocatalytic NH_3 synthesis. *ACS Sustain. Chem. Eng.* **2019**, 7, 12408-12418.

(5) Martyna, C.; Jędrzej, P.; Stefano, C.; Joanna, S.; Maciej, G. Photocatalysis in aqueous micellar media enables divergent C-H arylation and N-dealkylation of benzamides. *ACS Catal.* **2022**, 12, 3543-3549.

(6) Luo, L.; Xiao, X.; Li, Q.; Wang, S.; Li, Y.; Hou, J.; Jiang, B. Engineering of single atomic Cu-N_3 active sites for efficient singlet oxygen production in photocatalysis. *ACS Appl. Mater. Interfaces* **2021**, 13, 58596-58604.

(7) Zhu, S.; Liu, Y.; Chen, X.; Qu, L.; Yu, B. Polymerization-enhanced photocatalysis for the functionalization of C(sp^3)-H bonds. *ACS Catal.* **2022**, 12, 126-134.

(8) He, X.; Yao, X.; Cai, S.; Li, H.; He, L. Visible light-driven carbamoyloxylation of the α-C(sp^3)-H bond of arylacetones via radicaliniti-ated hydrogen atom transfer. *Chem. Commun.* **2022**, 58, 5845-5848.

(9) Lin, H.; Xu, Y.; Wang, B.; Li, D.; Zhou, T.; Zhang, J. Postsynthetic modification of metal-organic frameworks for photocatalytic applications. *Small Struct.* **2022**, 2100176.

(10) Yoshio, N.; Atsuko, Y. Generation and detection of reactive oxygen species in photocatalysis. *Chem. Rev.* **2017**, 117, 11302-11336.

(11) Megan, H.; Jack, T.; David, W. Photoredox catalysis in organic chemistry. *J. Org. Chem.* **2016**, 81, 6898-6926.

(12) Sun, K.; Shi, A.; Liu, Y.; Chen, X.; Xiang, P.; Wang, X.; Qu, L.; Yu, B. A general electron donor-acceptor complex for photoactivation of arenes via thianthrenation. *Chem. Sci.* **2022**, 13, 5659-5666.

(13) Wang, C.; Yi, X.; Wang, P. Powerful combination of MOFs and C_3N_4 for enhanced photocatalytic performance. *Appl. Catal. B Environ.* **2019**, 247, 24-48.

(14) Yang, Z.; Xiao, W.; Zhang, X.; Liao, S. Organocatalytic cationic degenerate chain transfer polymerization of vinyl ethers with excellent temporal control. *Polym. Chem.* **2022**, 13, 2776-2781.

(15) Zou, S.; Luo, X.; Chen, C.; Xi, C. Photoredox-catalyzed fluorodifluoroacetylation of alkenes with $FSO_2CF_2CO_2Me$ and $Et_3N{\cdot}3HF$. *Org. Biomol. Chem.* **2022**, 20, 3726-3730.

(16) Chen, R.; Chen, J.; Che, H.; Zhou, G.; Ao, Y.; Liu, B. Atomically dispersed main group magnesium on cadmium sulfide as the active site for promoting photocatalytic hydrogen evolution catalysis. *Chin. J. Struct. Chem*. **2022**, 41, 2201014-2201018.

(17) Cai, R.; Zhang, B.; Shi, J.; Li, M.; He, Z. Rapid photocatalytic decolorization of methyl orange under visible light using VS_4/carbon powder nanocomposites. *ACS Sustainable Chem. Eng.* **2017**, 5, 7690-7699.

(18) Li, X.; Dai, K.; Pan, C.; Zhang, J. Diethylenetriamine-functionalized CdS nanoparticles decorated on Cu_2S snowflake microparticles for photocatalytic hydrogen production. *ACS Appl. Nano Mater.* **2020**, 3, 11517-11526.

(19) Indrani, M.; Vatsala, C.; Raj, K. Sunlight-driven photocatalytic degradation of ciprofloxacin by carbon dots embedded in ZnO nanostructures. *ACS Appl. Nano Mater.* **2021**, 4, 7686-7697.

(20) Marco, P.; Fabrizio, S.; Simone, B.; Marco, Z.; Francesco, P.; Alessandra, B.; Valter, M. Assessing a photocatalytic activity index for TiO_2 colloids by controlled periodic illumination. *ACS Catal.* **2020**, 10, 9612-9623.

(21) Wang, J.; Wang, J.; Wang, W.; Wang, Y.; Hu, X.; Liu, J.; Gong, X.; Miao, W.; Ding, L.; Li, X.; Tang, J. Synthesis, modification and application of titanium dioxide nanoparticles: a review. *Nanoscale* **2022**, 14, 6709-6734.

(22) Reshma, B.; Srashti, J.; Chathakudath, P.; Santosh, K.; Satishchandra, O. Direct Z-Scheme g-C_3N_4/$FeWO_4$ nanocomposite for enhanced and selective photocatalytic CO_2 reduction under visible light. *ACS Appl. Mater. Interfaces* **2019**, 11, 6174-6183.

(23) Gao, M.; Feng, J.; Zhang, Z.; Gu, M.; Wang, J.; Zeng, W.; Lv, Y.; Ren, Y.; Wei, T.; Fan, Z. Wrinkled ultrathin graphitic C_3N_4 nanosheets for photocatalytic degradation of organic wastewater. *ACS Appl. Nano Mater.* **2018**, 1, 6733-6741.

(24) Martin, R.; Huo, P.; Marcel, Š.; Nela, A.; Ivana, T.; Lenka, M.; Jaroslav, L.; Ladislav, S.; Piotr, K.; Michal, R.; Petr, P.; Kamila, K. Novel TiO_2/C_3N_4 photocatalysts for photocatalytic reduction of CO_2 and for photocatalytic decomposition of N_2O. *J. Phys. Chem. A* **2016**, 120, 8564-8573.

(25) Zhang, Q.; Deng, J.; Xu, Z.; Mohamed, C.; Ma, D. High-efficiency broadband C_3N_4 photocatalysts: synergistic effects from upconversion and plasmons. *ACS Catal.* **2017**, 7, 6225-6234.

(26) Maryam, B.; Ferial, G.; Amirhassan, A.; Masoud, M. Metal-organic framework-based sorbents in analytical sample preparation. *Coord. Chem. Rev.* **2021**, 445, 214107.

(27) Li, H.; Wang, K.; Sun, Y.; Christina, T.; Li, J.; Zhou, H. Recent

advances in gas storage and separation using metal-organic frameworks. *Mater. Today* **2018**, 21, 108-121.

(28) Qiu, S.; Xue, M.; Zhu, G. Metal-organic framework membranes: from synthesis to separation application. *Chem. Soc. Rev.* **2014**, 43, 6116.

(29) Song, Q.; Yang, Y.; Yuan, F.; Zhu, S.; Wang, J.; Xiang, S.; Zhang, Z. Electrostatic force-driven lattice water bridging to stabilize a partially charged indium MOF for efficient separation of C_2H_2/CO_2 mixtures. *J. Mater. Chem. A* **2022**, 10, 9363-9369.

(30) Zhou, H.; Susumu, K. Metal-Organic Frameworks (MOFs). *Chem. Soc. Rev.* **2014**, 43, 5415-5418.

(31) Archisman, D.; Amita, S.; Wang, X.; Abhinav, K.; Liu, J. Luminescent sensing of nitroaromatics by crystalline porous materials. *CrystEngComm* **2020**, 22, 7736.

(32) Li, H.; Zhao, S.; Zang, S.; Liu, J. Functional metal-organic frameworks as effective sensors of gases and volatile compounds. *Chem. Soc. Rev.* **2020**, 49, 6364.

(33) Li, H.; Zhao, S.; Zang, S.; Liu, J. Metal-organic frameworks: functional luminescent and photonic materials for sensing applications. *Chem. Soc. Rev.* **2017**, 46, 3242.

(34) William, P.; Soumya, M.; Nathan, D.; Aamod, V.; Li, J.; Sujit, K. MOF-253-supported Ru complex for photocatalytic CO_2 reduction by coupling with semidehydrogenation of 1,2,3,4-tetrahydroisoquinoline (THIQ). *Inorg. Chem.* **2019**, 58, 16574-16580.

(35) Gong, Y.; Mei, J.; Liu, J.; Huang, H.; Zhang, J.; Li, X.; Zhong, D.; Lu, T. Manipulating metal oxidation state over ultrastable metal-organic frameworks for boosting photocatalysis. *Appl. Catal. B Environ.* **2021**, 292, 120156.

(36) Sanchita, K.; Soumitra, B.; Faruk, A.; Tapas, K. Covalent grafting of molecular photosensitizer and catalyst on MOF-808: effect of pore confinement toward visible light-driven CO_2 reduction in water. *Energy Environ. Sci.* **2021**, 14, 2429-2440.

(37) Liao, W.; Zhang, J.; Wang, Z.; Lu, Y.; Yin, S.; Wang, H.; Fan, Y.; Pan, M.; Su, C. Semiconductive amine-functionalized Co(II)-MOF for visible-light-driven hydrogen evolution and CO_2 reduction. *Inorg. Chem.* **2018**, 57, 11436-11442.

(38) Liu, J.; Chen, L.; Cui, H.; Zhang, J.; Zhang, L.; Su, C. Applications of metal-organic frameworks in heterogeneous supramolecular catalysis. *Chem. Soc. Rev.* **2014**, 43, 6011.

(39) Tang, Y.; Zhao, L.; Ji, G.; Zhang, Y.; He, C.; Wang, Y.; Wei, J.; Duan, C. Ligand-regulated metal-organic frameworks for synergistic photoredox and nickel catalysis. *Inorg. Chem. Front.* **2022**, DOI: 10.1039/d2qi00173j.

(40) Cao, L.; Wu, X.; Liu, Y.; Mao, F.; Shi, Y.; Li, J.; Zhu, M.; Dai, S.; Chen, A.; Liu, P.; Yang, H. Electrochemical conversion of CO_2 to syngas with a stable H_2/CO ratio in a wide potential range over ligand-engineered metal-organic frameworks. *J. Mater. Chem. A* **2022**, 10, 9954-9959.

(41) Huo, M.; Sun, T.; Wang, Y.; Sun, P.; Dang, J.; Wang, B.; Dharanipragada, N.; Inge, A.; Zhang, W.; Cao, R.; Ma, Y.; Zheng, H. A heteroepitaxially grown two-dimensional metal-organic framework and its derivative for the electrocatalytic oxygen reduction reaction. *J. Mater. Chem. A* **2022**, 10, 10408-10416.

(42) Li, Z.; Guo, X.; Qiu, J.; Lu, H.; Wang, J.; Lin, J. Recent advances in the applications of thoriumbased metal-organic frameworks and molecular clusters. *Dalton Trans*. **2022**, 51, 7376-7389.

(43) Yuan, M.; Chen, J.; Zhang, H.; Li, Q.; Zhou, L.; Yang, C.; Liu, R.; Liu, Z.; Zhang, S.; Zhang, G. Host-guest molecular interaction promoted urea electrosynthesis over a precisely designed conductive metal-organic framework. *Energy Environ. Sci.* **2022**, 15, 2084-2095.

(44) Zhao, H.; Pang, X.; Huang, Y.; Bai, Y.; Ding, J.; Bai, H.; Fan, W. Electrocatalytic reduction of 4-nitrophenol over Ni-MOF/NF: understanding the self-enrichment effect of H-bonds. *Chem. Commun.* **2022**, 58, 4897.

(45) Li, M.; Ye, C.; Li, Z.; Lin, Q.; Cao, J.; Liu, F.; Song, G.; Sibudjing, K. 1D confined materials synthesized *via* a coating method for thermal catalysis and energy storage applications. *J. Mater. Chem. A* **2022**, 10, 6330.

(46) Shi, J.; Teng, W.; Deng, Z.; Bruce, E.; Zhang, W. Pollutants transformation by metal nanoparticles in confined nanospaces. *Environ. Sci.: Nano* **2021**, 8, 3435.

(47) Lui, R.; Stephane, R.; Tian, M.; Ivan, D.; Simon, J.; Valeska, P. Manipulation of the crystalline phase diagram of hydrogen through nanoscale confinement effects in porous carbons. *Nanoscale* **2022**, 14, 7250.

(48) Xiong, M.; Wang, G.; Zhao, S.; Lv, Z.; Xing, S.; Zhang, J.; Zhang, B.; Qin, Y.; Gao, Z. Engineering of platinum-oxygen vacancy interfacial sites in confined catalysts for enhanced hydrogenation selectivity. *Catal. Sci. Technol*. **2022**, 12, 2411.

(49) Xu, Z.; Sarawoot, I.; Jia, X.; Wang, F.; Shen, Y.; Wang, P.; Zhang, D. SO_2-Tolerant catalytic reduction of NO_x by confining active species in TiO_2 nanotubes. *Environ. Sci.: Nano* **2022**, DOI: 10.1039/d2en00144f.

(50) Li, J.; He, L.; Liu, Q.; Ren, Y.; Jiang, H. Visible light-driven efficient palladium catalyst turnover in oxidative transformations within confined frameworks. *Nat. Commun.* **2022**, 13, 928.

(51) Cui, P.; Wang, P.; Zhao, Y.; Sun, W. Fabrication of desired metal-organic frameworks via postsynthetic exchange and sequential linker installation. *Cryst. Growth Des.* **2019**, 19, 1454-1470.

(52) Christina, T.; Qin, J.; Pang, J.; Yuan, S.; Benjamin, B.; Zhou, H. Interior decoration of stable Metal-Organic Frameworks. *Langmuir* **2018**, 34, 13795-13807.

(53) Pang, J.; Yuan, S.; Qin, J.; Wu, M.; Christina, T.; Li, J.; Huang, N.; Li, B.; Zhang, P.; Zhou, H. Enhancing pore-environment complexity using a trapezoidal linker: toward stepwise assembly of multivariate quinary Metal-Organic Frameworks. *J. Am. Chem. Soc.* **2018**, 140, 12328-12332.

(54) Pang, J.; Yuan, S.; Qin, J.; Christina, T.; Huang, N.; Li, J.; Wang, Q.; Wu, M.; Yuan, D.; Hong, M.; Zhou, H. Tuning the ionicity of stable Metal-Organic Frameworks through ionic linker installation. *J. Am. Chem. Soc.* **2019**, 141, 3129-3136.

(55) Yuan, S.; Chen, Y.; Qin, J.; Lu, W.; Zou, L.; Zhang, Q.; Wang, X.; Sun, X.; Zhou, H. Linker installation: engineering pore environment with precisely placed functionalities in zirconium MOFs. *J. Am. Chem. Soc.* **2016**, 138, 8912-8919.

(56) Pang, J.; Di, Z.; Qin, J.; Yuan, S.; Christina, T.; Li, j.; Zhang, P.; Wu, M.; Yuan, D.; Hong, M.; Zhou, H. Precisely embedding active sites into a mesoporous Zr-framework through linker installation for high-efficiency photocatalysis. *J. Am. Chem. Soc.* **2020**, 142, 15020-15026.

(57) Qiao, G.; Yuan, S.; Pang, J.; Rao, H.; Christina, T.; Dang, D.; Qin, J.; Zhou, H.; Yu, J. Functionalization of zirconium-based metal-organic layers with tailored pore environments for heterogeneous catalysis. *Angew. Chem. Int. Ed*. **2020**, 59, 18224-18228.

(58) Carlos, M.; André, D.; Susana, R.; Isabel, C.; Baltazar, D.; Luís, C.; Salete, S. Oxidative catalytic versatility of a trivacant polyoxotungstate incorporated into MIL-101(Cr). *Catal. Sci. Technol.* **2014**, 4, 1416.

(59) Li, Y.; Gao, Q.; Zhang, L.; Zhou, Y.; Zhong, Y.; Ying, Y.; Zhang, M.;

Huang, C.; Wang, Y. $H_5PV_2Mo_{10}O_{40}$ encapsulated in MIL-101(Cr): facile synthesis and characterization of rationally designed composite materials for efficient decontamination of sulfur mustard. *Dalton Trans*. **2018**, 47, 6394.

(60) Mialane, P.; Mellot-Draznieks, C.; Gairola, P.; Duguet, M.; Benseghir, Y.; Oms, O.; Dolbecq, A. Heterogenisation of polyoxometalates and other metal-based complexes in metal-organic frameworks: from synthesis to characterisation and applications in catalysis. *Chem. Soc. Rev*. **2021**, 50, 6152.

(61) Sun, J.; Sara, A.; Pascal, V.; Liu, Y.; Karen, L. POM@MOF hybrids: synthesis and applications. *Catalysts* **2020**, 10, 578.

(62) Yuan, M.; Sun, C.; Liu, Y.; Lu, Y.; Zhang, Z.; Li, X.; Tian, H.; Zhang, S.; Liu, S. Synthesis, characterization, and property investigation of a Metal-Organic Framework encapsulated polyoxometalate guests: an advanced inorganic chemistry experiment. *J. Chem. Educ.* **2020**, 97, 4152-4157.

(63) Zhang, S.; Ou, F.; Ning, S.; Cheng, P. Polyoxometalate-based metal-organic frameworks for heterogeneous catalysis. *Inorg. Chem. Front*. **2021**, 8, 1865.

(64) Youven, B.; Alex, L.; Mathis, D.; Pierre, M.; Maria, G.; Catherine, R.; Thomas, P.; Minh-Huong, H.; Mohamed, H.; Marc, F.; Anne, D.; Capucine, S.; Caroline, M. Co-immobilization of a Rh catalyst and a Keggin polyoxometalate in the UiO-67 Zr-based Metal-Organic Framework: in depth structural characterization and photocatalytic properties for CO_2 reduction. *J. Am. Chem. Soc.* **2020**, 142, 9428-9438.

(65) Cui, B.; Fu, G. Process of metal-organic framework (MOF)/covalent-organic framework (COF) hybrids-based derivatives and their applications on energy transfer and storage. *Nanoscale* **2022**, 14, 1679.

(66) Guo, C.; Duan, F.; Zhang, S.; He, L.; Wang, M.; Chen, J.; Zhang, J.; Jia, Q.; Zhang, Z.; Du, M. Heterostructured hybrids of metal-organic frameworks (MOFs) and covalent-organic frameworks (COFs). *J. Mater. Chem. A* **2022**, 10, 475.

(67) Sun, D.; Dong-Pyo, K. Hydrophobic MOFs@metal nanoparticles@COFs for interfacially confined photocatalysis with high efficiency. *ACS Appl. Mater. Interfaces* **2020**, 12, 20589-20595.

(68) Tang, H.; Sun, X.; Zhang, F. Development of MOF-based heterostructures for photocatalytic hydrogen evolution. *Dalton Trans*. **2020**, 49, 12136.

(69) Zhang, H.; Yang, Y.; Li, C.; Tang, H.; Zhang, F.; Zhang, G.; Yan, H. A new strategy for constructing covalently connected MOF@COF core-shell heterostructures for enhanced photocatalytic hydrogen evolution. *J. Mater. Chem. A* **2021**, 9, 16743.

(70) Zhang, M.; Li J.; Wang, R.; Zhao, S.; Zang, S.; Thomas, C. Construction of core-shell MOF@COF hybrids with controllable morphology adjustment of COF shell as a novel platform for photocatalytic cascade reactions. *Adv. Sci.* **2021**, 8, 2101884.

(71) Kayhaneh, B.; Ali, M. The role of metal-organic porous frameworks in dual catalysis. *Inorg. Chem. Front.* **2021**, 8, 3618.

(72) Chen, L.; Qi, Z.; Peng, X.; Chen, J.; Pao, C,.; Zhang, X.; Dun, C.; Melissa, Y.; David, P.; Jeffrey, J.; Guo, J.; Gabor, A.; Su, J. Insights into the mechanism of methanol steam reforming tandem reaction over CeO_2 supported single-site catalysts. *J. Am. Chem. Soc*. **2021**, 143, 12074-12081.

(73) Fu, J.; Yang, Y.; Hu, J. Dual-sites tandem catalysts for C-N bond formation via electrocatalytic coupling of CO_2 and nitrogenous small molecules. *ACS Materials Lett.* **2021**, 3, 1468-1476.

(74) Li, Z.; Cheng, H.; Zhang, X.; Ji, M.; Wang, S.; Wang, S. The comparative study on the catalytic activity of Cu-M/$Ce_{0.8}Zr_{0.2}O_2$ (M = W, Nb, Cr and Mo) catalysts with dual-function for the simultaneous removal of NO and CO under oxygen-rich conditions. *Catal. Sci. Technol.* **2021**, 11, 4987.

(75) Nilanjan, S.; Athulya, S.; Manpreet, S.; Ranadip, G.; Renjith, S.; Subhadip, N. Chemically robust and bifunctional Co(II)-framework for trace detection of assorted organo-toxins and highly cooperative Deacetalization-Knoevenagel condensation with pore-fitting-induced size-selectivity. *ACS Appl. Mater. Interfaces* **2021**, 13, 28378-28389.

(76) Zhang, Y.; Huang, C.; Mi, L. Metal-organic frameworks as acid- and/or base-functionalized catalysts for tandem reactions. *Dalton Trans*. **2020**, 49, 14723.

(77) Shi, W.; Quan, Y.; Lan, G.; Ni, K.; Song, Y.; Jiang, X.; Wang, C.; Lin, W. Bifunctional metal-organic layers for tandem catalytic transformations using molecular oxygen and carbon dioxide. *J. Am. Chem. Soc.* **2021**, 143, 16718-16724.

(78) Jin, J.; Wu, K.; Liu, X.; Huang, G.; Huang, Y.; Luo, D.; Xie, M.; Zhao, Y.; Lu, W.; Zhou, X.; He, J.; Li, D. Building a pyrazole-benzothiadiazole-pyrazole photosensitizer into Metal-Organic Frameworks for photocatalytic aerobic oxidation. *J. Am. Chem. Soc*. **2021**, 143, 21340-21349.

(79) Christian, F.; James, N.; Rebecca, S.; Zhang, X.; Hu, Y.; Yang, S.; Huang, J.; Zhang, J. Symmetry-guided synthesis of *N,N'*-bicarbazole and porphyrin-based mixed-ligand Metal-Organic Frameworks: light harvesting and energy transfer. *J. Am. Chem. Soc.* **2021**, 143, 20411-20418.

(80) Liu, J.; Li, Q.; Xiao, X.; Li, F.; Zhao, C.; Sun, Q.; Qiao, P.; Zhou, J.; Wu, J.; Li, B.; Bao, H.; Jiang, B. Metal-organic frameworks loaded on phosphorus-doped tubular carbon nitride for enhanced photocatalytic hydrogen production and amine oxidation. *J. Colloid. Interf. Sci.* **2021**, 590, 1-11.

(81) Wang, S.; Tang, L.; Cai, B.; Yin, Z.; Li, Y.; Xiong, L.; Kang, X.; Xuan, J.; Pei, Y.; Zhu, M. Ligand modification of Au_{25} nanoclusters for near-Infrared photocatalytic oxidative functionalization. *J. Am. Chem. Soc.* **2022**, 144, 3787-3792.

(82) Liu, S.; Li, Y.; Ding, K.; Chen, W.; Zhang, Y.; Lin, W. Mechanism on carbon vacancies in polymeric carbon nitride for CO_2 photoreduction. *Chin. J. Struct. Chem.* **2020**, 39, 2068-2076.

(83) Md., I.; Raffaele, C.; Gianluca, M.; Luca, N.; Matteo, M. Mechanistic and multiscale aspects of thermocatalytic CO_2 conversion to C1 products. *Catal. Sci. Technol.* **2021**, 11, 6601.

(84) Dao, X.; Sun, W. Single- and mixed-metal-organic framework photocatalysts for carbon dioxide reduction. *Inorg. Chem. Front.* **2021**, 8, 3178.

(85) Sourav, G.; Arindam, M.; Arnab, S.; Kanika, K.; Subhra, J. Recent progress in materials development for CO_2 conversion: issues and challenges. *Mater. Adv.* **2021**, 2, 3161.

(86) Ma, D.; Jin, T.; Xie, K.; Huang, H. An overview of flow cell architecture design and optimization for electrochemical CO_2 reduction. *J. Mater. Chem. A* **2021**, 9, 20897.

(87) Siglinda, P.; Kevin, M.; Guy, B.; Gabriele, C. Reuse of CO_2 in energy intensive process industries. *Chem. Commun.* **2021**, 57, 10967.

(88) Xiong, J.; Zhang, M.; Lu, M.; Zhao, K.; Han, C.; Cheng, G.; Wen, Z. Achieving simultaneous Cu particles anchoring in meso-porous TiO_2 nanofabrication for enhancing photo-catalytic CO_2 reduction through rapid charge separation. *Chin. Chem. Lett.* **2022**, 33, 1313-1316.

(89) Fu, S.; Yao, S.; Guo, S.; Guo, G.; Yuan, W.; Lu, T.; Zhang, Z. Feeding carbonylation with CO_2 via the synergy of single-site/nanocluster catalysts in a photosensitizing MOF. *J. Am. Chem. Soc*. **2021**, 143, 20792-20801.

(90) Yun, Y.; Sheng, H.; Bao, K.; Xu, L.; Zhang, Y.; Didier, A.; Zhu, M. Design and remarkable efficiency of the robust sandwich cluster compo-

DOI: 10.14102/j.cnki.0254-5861.2022-0140

site nanocatalysts ZIF-8@Au25@ZIF-67. *J. Am. Chem. Soc.* **2020**, 142, 4126-4130.
(91) Khan, I. S.; Mateo, D.; Shterk, G.; Shoinkhorova, T.; Poloneeva, D.; Garzon-Tovar, L.; Gascon, J. An efficient metal-organic framework-derived nickel catalyst for the light driven methanation of CO_2. *Angew. Chem. Int. Ed*. **2021**, 60, 26476-26482.
(92) Chen, E.; Qiu, M.; Zhang, Y.; He, L.; Sun, Y.; Zheng, H.; Wu, X.; Zhang, J.; Lin, Q. Energy band alignment and redox-active sites in metalloporphyrin-spaced metal-catechol frameworks for enhanced CO_2 photoreduction. *Angew. Chem. Int. Ed*. **2022**, 61, e202111622.
(93) Ana, A.; Sara, R.; Iv´an, O.; Ana, T.; Marta, L.; Fabrice, S.; Daniel, A.; Sara, B.; David, Á.; Patricia, H. Ultrafast reproducible synthesis of a Agnanocluster@MOF composite and its superior visible-photocatalytic activity in batch and in continuous flow. *J. Mater. Chem. A* **2021**, 9, 15704.
(94) Ajay, L.; Anil, M. Reduced graphene oxide-decorated CdS/ZnO nanocomposites for photoreduction of hexavalent chromium and photodegradation of methylene blue. *Dalton Trans*. **2021**, 50, 14163.
(95) Ayushi, S.; Ashish, K.; Liu, J.; Abhinav, K. Syntheses, design strategies, and photocatalytic charge dynamics of metal-organic frameworks (MOFs): a catalyzed photo-degradation approach towards organic dyes. *Catal. Sci. Technol.* **2021**, 11, 3946.
(96) Bui, T.; Nguyen, V.; Nguyen, T. The development of biomass-derived carbonbased photocatalysts for the visible-light-driven photodegradation of pollutants: a comprehensive review. *RSC Adv*. **2021**, 11, 30574.
(97) Zhang, B.; He, X.; Yu, C.; Liu, G.; Ma, D.; Cui, C.; Yan, Q.; Zhang, Y.; Zhang, G.; Ma, J.; Xin, Y. Degradation of tetracycline hydrochloride by ultrafine TiO_2 nanoparticles modified g-C_3N_4 heterojunction photocatalyst: influencing factors, products and mechanism insight. *Chin. Chem. Lett.* **2022**, 33, 1337-1342.
(98) Xia, Z.; Shi, B.; Zhu, W.; Lü, C. Temperature-responsive polymer-tethered Zr-porphyrin MOFs encapsulated carbon dot nanohybrids with boosted visible-light photodegradation for organic contaminants in water. *Chem. Eng. J.* **2021**, 426, 131794.
(99) Wang, J.; Cao, C.; Wang, J.; Zhang, Y.; Zhu, L. Insights into highly efficient photodegradation of poly/perfluoroalkyl substances by In-MOF/BiOF heterojunctions: built-in electric field and strong surface adsorption. *Appl. Catal. B Environ.* **2022**, 304, 121013.
(100) Chen, P.; He, X.; Pang, M.; Dong, X.; Zhao, S.; Zhang, W. Iodine capture using Zr-based Metal-Organic Frameworks (Zr MOFs): adsorption performance and mechanism. *ACS Appl. Mater. Interfaces* **2020**, 12, 20429-20439.
(101) Gao, K.; Li, H.; Meng, Q.; Wu, J.; Hou, H. Efficient and selective visible-light-driven oxidative coupling of amines to imines in air over CdS@Zr-MOFs. *ACS Appl. Mater. Interfaces* **2021**, 13, 2779-2787.
(102) Huang, G.; Chen, J.; Huang, Y.; Wu, K.; Luo, D.; Jin, J.; Zheng, J.; Xu, S.; Lu, W. Mixed-linker isoreticular Zn(II) metal-organic frameworks as Brønsted acid-base bifunctional catalysts for Knoevenagel condensation reactions. *Inorg. Chem.* **2022**, DOI:10.1021/acs.inorgchem.2c00941.
(103) Tang, D.; Yang, X.; Wang, B.; Ding, Y.; Xu, S.; Liu, J.; Peng, Y.; Yu, X.; Su, Z.; Qin, X. One-step electrochemical growth of 2D/3D Zn(II)-MOF hybrid nanocomposites on an electrode and utilization of a PtNPs@2D MOF nanocatalyst for electrochemical immunoassay. *ACS Appl. Mater. Interfaces* **2021**, 13, 46225-46232.
(104) Yuan, S.; Qin, J.; Xu, H.; Su, J.; Daniel, R.; Chen, Y.; Zhang, L.; Christina, L.; Wang, Q.; Son, D.; Xu, H.; Huang, Z.; Zou, X.; Zhou, H. [$Ti_8Zr_2O_{12}(COO)_{16}$] cluster: an ideal inorganic building unit for photoactive metal-organic frameworks. *ACS Cent. Sci.* **2018**, 4, 105-111.
(105) Ha, L.; Thanh, T.; Dinh, L.; Tan, L.; Viet, Q.; Nam, T. A Titanium-organic framework: engineering of the band-gap energy for photocatalytic property enhancement. *ACS Catal*. **2017**, 7, 338-342.
(106) Vieira, C.; Maurin, G.; Leitão, A. Computational exploration of the catalytic degradation of sarin and its simulants by a titanium metal-organic framework. *J. Phys. Chem. C* **2019**, 123, 19077-19086.

Received: May 27, 2022
Accepted: June 12, 2022
Published online: June 20, 2022
Published: October 31, 2022

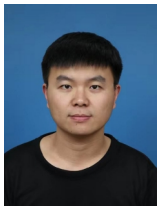

Hao Zhang received his bachelor's degree from Yantai University in 2019. In the same year, he was admitted to the Shandong Provincial Key Laboratory of Chemical Energy Storage and Novel Cell Technology of Liaocheng University for his master's degree. His current research focuses on molecular complexes and MOFs materials in photocatalytic decomposition of water to produce hydrogen and catalytic conversion of small organic molecules.

Ru Sun graduated from Taishan University with a bachelor's degree. She is currently studying in the Shandong Provincial Key Laboratory of Chemical Energy Storage and Novel Cell Technology of Liaocheng University under the guidance of Prof. Da-Cheng Li. Her main research interests are the synthesis and properties of functionalized POMs.

Da-Cheng Li graduated from Liaocheng University and obtained the bachelor's degree in 1985. From 1989 to 1991, he studied in the graduate program of analytical chemistry at Shaanxi Normal University. He now works at the Shandong Provincial Key Laboratory of Chemical Energy Storage and Novel Cell Technology of Liaocheng University. In recent years, he has been engaged in the research of borane chemistry, crown ether chemistry, coordination chemistry, drug polycrystal and eutectic.

Jian-Min Dou received his bachelor's degree from Liaocheng University in 1986 and earned his Ph.D. degree at Fudan University in 1998. He has been teaching in Liaocheng University for more than 30 years. His previous research focused on the structure and magnetic properties of metal crown ethers. The current direction is related to energy catalysis including photocatalytic water decomposition, CO_2 reduction and degradation of organic pollutants.

DOI: 10.14102/j.cnki.0254-5861.2022-0140